Journal of Low Temperature Physics, Vol. 76, Nos. 3/4, 1989

Microcalorimetry Study of the Monolayer ^{4}He Ordering Transition on Single Crystal Graphite

H. B. Chae* and Michael Bretz

Department of Physics, University of Michigan, Ann Arbor, Michigan

(Received February 8, 1989)

We have developed a low-temperature, ac microcalorimeter for exploring adsorption on a single 2.25 mm^2 graphite leaf that is capable of 10 picoJoule/degree resolution. The microcalorimeter was used to determine the phase diagram and heat capacity critical exponents α of monolayer ^{4}He films at the commensurate ordering transition. After in situ baking at 600 K, we reproduced the narrow-ordered phase region ($\simeq$1% in coverage) reported by Campbell and Bretz for HOPG, but find quasilogarithmic, rather than power law, heat capacity divergences. We argue that the disappearance of the Potts-like exponent in the heat capacity is attributable to the geometry of nucleation along cleavage edge planes present on single crystal graphite surfaces.

1. INTRODUCTION

Since its discovery in 1971, the ordering transition of helium adsorbed on basal plane graphite[1] has been of considerable interest to adsorption researchers (Fig. 1). First thought to reflect an Ising lattice gas transition because of its apparent logarithmic peak shape when measured on Grafoil,[1] latter work demonstrated that when adsorbed on the much better quality *ZYX* graphite,† a strong power law divergence resulted.[2] This observation led to a reinterpretation of the ordered phase as a $\sqrt{3} \times \sqrt{3}$ R30° commensurate 2D solid, representing the first experimental analog of the theoretical 3-state Potts Model in 2 dimensions.[3]

*Present address: Thermophysics Division, National Institute of Standards and Technology, Gaithersburg, Maryland 20899.

†Grafoil, graphite foam and ZYX are exfoliated graphites and HOPG is a highly oriented pyrolytic graphite, all manufactured by Union Carbide, New York, New York.

0022-2291/89/0800-0199$06.00/0

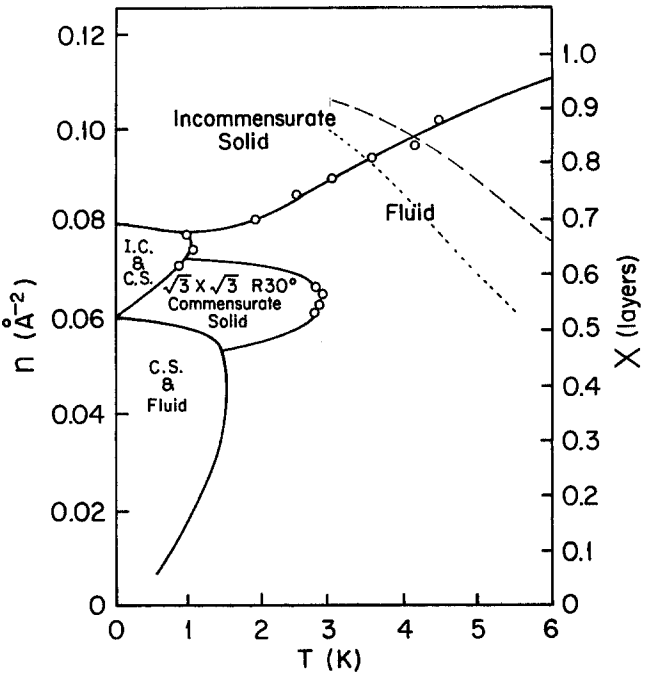

Fig. 1. Monolayer phase diagram of ^{4}He on graphite (from Ref. 4). Dotted line estimate 1% film depletion and dashed line bounds high-temperature region of ac calorimeter breakdown.

The recent ac microcalorimetry work of Campbell and Bretz[4] (hereafter referred to as CB) was designed to probe further possible heat capacity features on still better graphite substrates. CB constructed a microcalorimeter from a cleaved leaf of HOPG[2] and for the first time obtained adsorbed film heat capacity measurements on nonexfoliated graphite surfaces. Two results were obtained: the phase diagram of the commensurate phase was shown to be much narrower than for the exfoliates (Fig. 1), and at the critical coverage, $n_c = 0.0635/\text{Å}^2$, an asymmetric ordering heat capacity peak was observed with critical exponent $\alpha = 0$ for T below the critical temperature, T_c, and $\alpha \simeq 1/3$ (Potts-like) above T_c. They interpreted the narrow-ordered phase region as reflecting the excellent film geometry of HOPG and the unexpected nonuniversality as caused by residual impurity, rather than size-limiting effects.

We have improved on the CB calorimeter design and re-explored the ordered phase region. Our improvements were to switch to a natural single graphite crystal, since there is scanning microscope evidence from gold

decorated surfaces that many fewer step planes exist on single crystals than on HOPG,[5] and to construct the cell so that higher bakeout temperatures were possible than CB's 170°C.

In this article we describe in detail cell construction, experimental apparatus and acquisition techniques, and report on three sets of runs (I, II and III) which give sequentially better data and clearer interpretations of the ^{4}He ordering transition. We analyze most of our resulting ordering peaks for their critical properties, finding all to be more or less logarithmic in shape. Those of Set II clearly result from a monolayer or two of underlayer impurity, while the peaks of Set III on single crystals of graphite, indicate that ordering nucleates outward from surface step planes which, if few enough in number, constrain the transition to be quasi-Ising-like.

2. AC THERMOMETRY[4]

We used the steady-state ac calorimetry technique developed by Sullivan and Seidel for measuring small samples.[6] A sample with internal heat capacity C_s and thermal conductance K_s communicates with the temperature bath T_b through a weak thermal link having conductance K_b. We choose a heater and thermometer which maximized contact conductances K_H and K_G and minimized the heat capacities C_H and C_G. Applying an ac voltage of frequency $\omega/2$ to the heater raises the sample above T_b, where it oscillates about a steady-state offset temperature. The rms magnitude of these oscillations T_{ac} depends on ω, the thermal time constants, and the sample heat capacity C_s, through the relation

$$T_{ac} = (P/\sqrt{2}\omega C_s)[1+(\omega\tau_1)^{-2}+(\omega\tau_2)^2]^{-1/2} \tag{1}$$

Here, P is the peak power to the ac heater (at frequency ω and $\tau_1 = C_s/K_b$ and τ_2 are the weak link and effective internal cell time constants, respectively. T_{ac} shifts out of phase, with respect to the heater oscillations, by an amount

$$\gamma \simeq \arctan\{[(\omega\tau_1)^{-1} - \omega\tau_2]^{-1}\} \tag{2}$$

One always measures the frequency profile to determine an operating frequency within a "plateau" region where neither τ_1 nor τ_2 dominates T_{ac}. For frequencies on the plateau, Eq. (2) simplifies to

$$T_{ac} \simeq P/[\sqrt{2}\omega C_s] \tag{3}$$

so the heat capacity C_s can be easily calculated. In practice, the weak link,

heater, thermometer, and addenda must be chosen carefully to match the thermal diffusion lengths, $l=(2\kappa/\omega\rho C)^{1/2}$, of each material of the ac cell (where ρ is density, κ is thermal conductivity, and C is the specific heat). The appropriate operating frequency can be determined by scanning ωT_{ac} and can be maintained by monitoring C to ensure that one has not shifted off the plateau.

3. CELL CONSTRUCTION AND OPERATION

Our redesigned ac calorimeter for exploring adsorbed films on single graphite surfaces is an advance over the previous HOPG calorimeter of Campbell and Bretz.[4] We used a single natural graphite leaf as a substrate. Instead of a dot of carbon paint, the thermometer and heater were vapor-deposited germanium films, permitting higher baking temperatures for the calorimeter and avoiding deposition of organic contaminates from the carbon binder onto the bare graphite surface. Details of cell construction are shown in Fig. 2a.

Graphite leaves were cleaved from Ticonderoga graphite using Scotch tape and cut into 1.5 mm × 1.5 mm × 1.5 mm × 3 μm squares. Large scale step features of the cleaving process were monitored with a Sloan Dektak II surface scanner Sloan Technology, Santa Barbara, California). We consistently found island sizes of 30 μm to 40 μm bounded by steps of about 1 μm in height.

We first vapor-deposited insulating SiO layers on one side of the graphite leaves. Unfortunately, electrical shorting occurred between the subsequently deposited germanium films and the graphite substrates, no matter how thick the SiO layers were, even up to 5000 Å. To circumvent the problem of occasional shorts grounding out heater/thermometers, we deposited a large number of germanium squares on top of the SiO and then chose the best ones. We used a Cu grid of 100 lines/in. for a mask, through which a 9 mil × 9 mil Ge matrix was deposited over the 5000 Å SiO layers on each cell we constructed. Electrical contacts were Ag tabs evaporated through a 4 mil × 4 mil grid positioned exactly on top of the germanium squares (see Fig. 2a). This procedure gave us a total of a hundred or so heaters/thermometers with dimensions of 1 mil × 4 mil on each graphite leaf. Grounding points were constructed by occasionally removing a grid wire in the Ag mask. After all depositions were made, electrical integrity was checked using a DVM with needle probes and the best calorimeter leaf was chosen. Good heater and thermometer elements about 1 mm apart were selected on that leaf and 1/2 mil NbTi leads (which are superconducting below about 10 K) were attached to the tabs with 1 mil beads of Ag epoxy. The other ends went to a stainless feedthrough via crimped gold pins. The

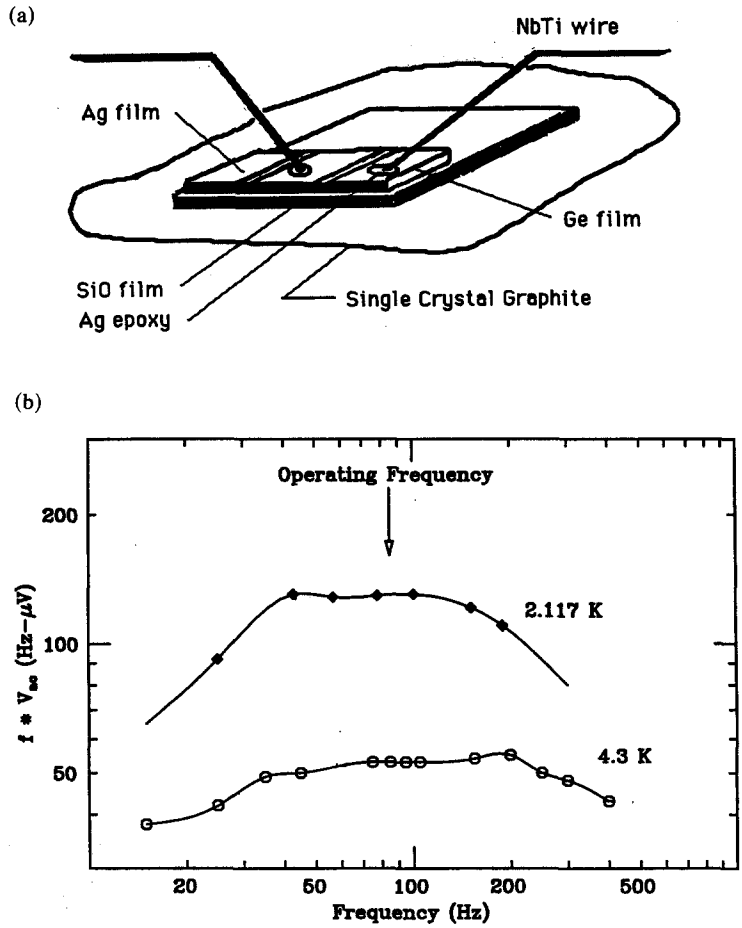

Fig. 2. (a) Schematic of cell construction on ≈2.25 mm^2 natural graphite leaf showing a few of the 100 or so germanium squares. (b) Frequency × ac voltage plotted vs. driving frequency.

finished single leaf graphite calorimeter had all addenda on one surface, leaving the opposite side bare for gas adsorption. It was free-standing with only the electrical leads supporting the leaf.

Care and practice were needed to obtain germanium films with the right resistance R and the appropriate temperature resistivity coefficient $d(\ln R)/dT$ at 4 K. Since Ge films grown on room-temperature substrates are amorphous, the low-temperature resistivity diverges, while films deposited on 450°C substrates anneal quickly, producing little temperature dependence to the resistivity. By extensive trial and error, along with 300 K, 77 K, and 4 K resistivity measurements, we determined that a substrate

temperature of 250°C and a deposition speed of 5 Å/sec were optimal for our needs. These conditions produced Ge films of about 100 kΩ and a temperature coefficient of over 50%/K at 4 K (see Ref. 7 for details. Studies of germanium film properties can be found in Ref. 8).

The assembled calorimeter, mounted on the stainless rotatable flange, was attached via a copper gasket to the copper, Grafoil-filled cell chamber described in Ref. 4. A 1.6 mm OD fill line lead from room temperature to a 6.1 mm shut-off valve at the top of the experimental chamber in the ^{3}He cryostat. Carbon resistors were mounted on the cryostat ^{4}He pot and on the ^{3}He pot to which the chamber was attached. These resistors, along with the calorimeter germanium heater and thermometer, were calibrated on several occasions with a 1000 mm/Hg Baratron pressure gauge using the vapor pressure of the helium bath, the T-58 temperature scale* and the EPT-76 corrections to it.† All resistors could be fit to

$$T(R) = A^2 \log(R - R_0)/(\log(R - R_0) - B)^2 \tag{4}$$

to within a few millidegrees over the 2.5 K to 4.5 K calibration range (A, B, and R_0 are constants).

The electrical configuration is shown in Fig. 3. A Z80-based microcomputer (Z2D System Two, Cromemco, Inc., Mountain View, Californa) was interfaced to the experiment with a 16 channel, 12-bit analog-to-digital converter board using 0–10 V (least significant bit = 2.44 mV). The background temperature of the cell was stablilized and measured with the ^{3}He pot heater, an ac bridge circuit and a bath mounted 20 KΩ metal film reference resistor. Temperature resolution was 15 μK at 3 K and computer-controlled stabilization was within 100 μK. The ac thermometer was biased with a 1.345 V mercury battery through a 17.5 MΩ metal film resistor. This provided a dc temperature-dependent offset to the cell of not more than 200 mK at the lowest temperatures of interest. Voltages for the ac thermometry were monitored using a vector lock-in amplifier (Model 393 Dynatrac, Ithaco Inc., Ithaca, New York), referenced to a heater oscillator in the 2f mode. The ac heater power was determined using two lock-in detectors and a bath-cooled, 754 kW reference metal film resistor connected in a four wire hookup to the superconducting cell heater leads. All experimental values, including the phase angle for the vector lock-in, were averaged over 50 sequential measurements, then recorded and offsets, heat capacities and temperatures were calculated.

Before packaging and cooldown, the cell capsule was evacuated through its shut-off valve by an Alcatal leak detector. The cell was baked to over

*The 1958 ^{4}He Scale of Temperatures, National Bureau of Standards, Monograph 10 (1960).
†The 1976 Provisional 0.5 K to 30 K Temperature Scales, Bur. Int. poids. Meas. (France).

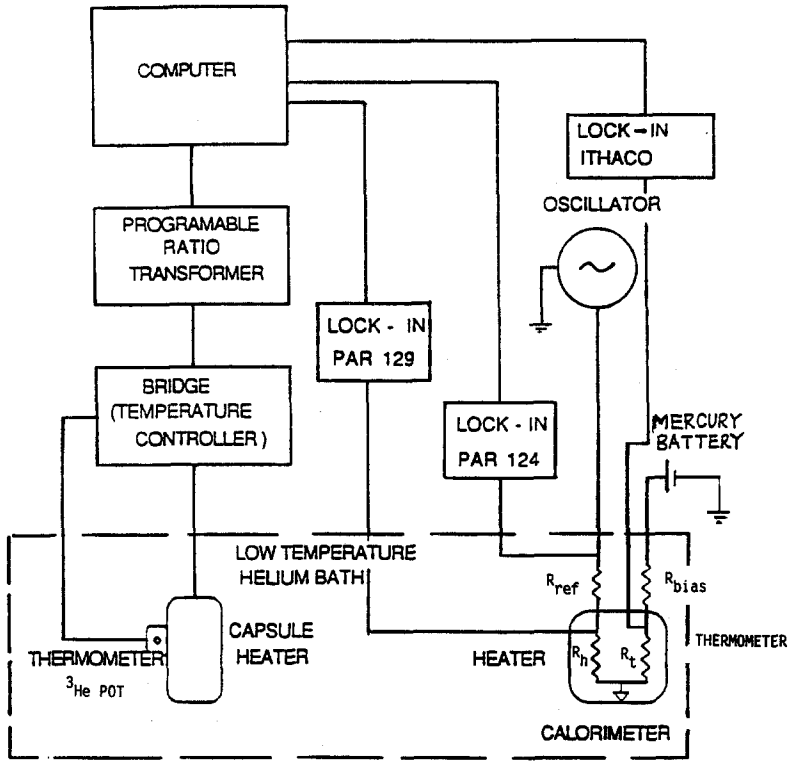

Fig. 3. Electronic diagram of cell bias and drive voltage, amplification and computer control.

280°C at 10^{-5} torr for 24 hours. The cell thermometer was calibrated at several elevated temperatures and was found reproduceable to within 3 Ω upon cooling back to room T (672 Ω). After cooldown, but before admitting gas to the cell, frequency response scans were taken at 4.3 K and 2.117 k, as shown in Figure 2b. Frequency independent plateaus were found at both temperatures, and we decided to operate at 85 Hz for all measurements. ac voltage signals at 85 Hz in this temperature range were 0.65 μV to 1.4 μV, as determined from the figure.

For coverage determinations, we took the results of a ^{4}He adsorption isotherm at 4.3 K made previously for the Grafoil ballast.[4] There, the point "B" method was used to determine a monolayer completion value of 16 ccSTP. Since the ac calorimeter surface area is a negligible fraction of the total graphite surface area, we assumed that the Grafoil and single leaf graphite surfaces coexist at the same coverage, given identical temperatures.

Later, when ordering peaks were located, we corrected our coverage determinations accordingly.

4. EXPERIMENTAL RESULTS

4.1. The Set I and Set II Data

Data were taken in three separate extensive runs denoted as sets I, II, and III. Set I was exploratory in nature. Only rough thermometer calibrations were taken and an empty calorimeter heat capacity value of about 6 nJ/K was measured at 4.2 K. This value is in agreement with the 4 nJ/K expected for out 10^{-5} cc of graphite[9] and 2.7 nJ/K calculated for the cell addenda.[7] Six weeks were spent in trying to locate the adsorbed ^{4}He ordering peak expected for a monolayer areal density of about 0.0625/Å^2. Some difficulty was, in fact, expected, since the ordering region is extremely narrow and coverage changes of just a few percent are enough to completely straddle it. The ordering transition finally appeared as a 0.3 nJ/K "bump" near 2.8 K on an otherwise steep, uniform heat capacity background (of 2.5 nJ/K at 2.8 K). From the (1.5 mm)^2 of graphite exposed leaf, we would expect the ideal 2D classical gas signature of the adsorbed ^{4}He to be about 0.18 nJ/K (assuming no ordering takes placed for adsorbates on the amorphous coating of the reverse side). Our observed peak, then, is about 1 Boltzmann in size, in agreement with the previous graphite leaf measurements of CB. Figure 4 gives a daily log indicating dates and coverages where this and other ordering peaks were observed for data Sets I, II, and III (coverages are in Torr as measured in our gas handling manifold).

After analyzing several runs, we determined that computer software changes were necessary to obtain data of sufficient quality for critical analysis. We therefore warmed the cryostat to LN_2 temperatures and pumped out the cell. After two weeks of changes and leak-checking, the experiment was again cooled, and the identical coverage of ^{4}He gas was reinserted into the cell. The ordering peak appeared just where expected in coverage, so we made an extensive two-week long coverage-temperature study, called Set II, in the vicinity of the ordering peak. At the end of Set II, a careful temperature calibration of resistors and heater was taken and all data reanalyzed.

Occasionally, we found that when coverage was changed, even by only 0.25%, the ordering peak vanished from the monotonic background heat capacity, later to reappear again at the next coverage increment. After pinpointing this problem to inadequate film annealing, we followed a conservative procedure for each coverage change: the cell remained above 10 K (but always less than 12 K) for 3 or 4 hours, followed by a 2-hour

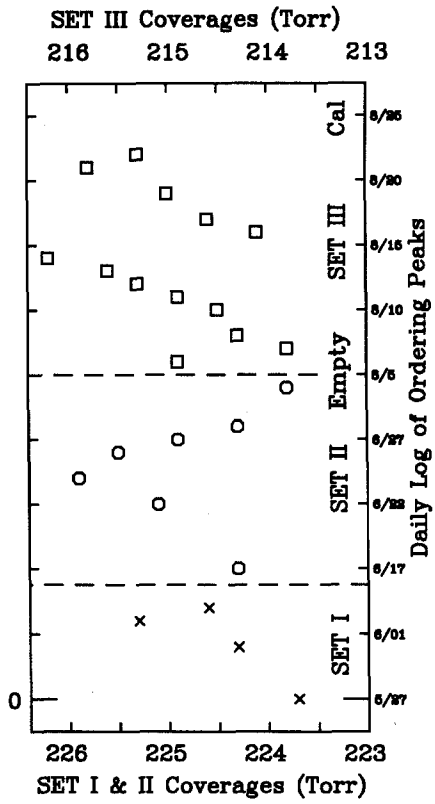

Fig. 4. Daily Log of ordering peak observations taken in 1986. Monolayer coverage = 389 Torr (16 ccSTP).

uniform cooldown to 4.2 K and a slow data taking, without any excessive heating spikes, while lowering T still further. Since the no-peak films were evidently off very slightly from the ordering coverage region, and since we did not have a reliable empty calorimeter run, a polynomial fit to a no-peak run was instead subtracted from all three-point-averaged data of Set II. (We shall present total heat capacity curves and further discuss the empty calorimeter situation in our analysis of the Set III data.)

4.2. Analysis of the Set II Data

The result of our Set II data subtraction procedures comprise Fig. 5. Considerable effort went into determining peak shape. We attempted to fit the data on each side of the peak, for each run of the set, with the standard

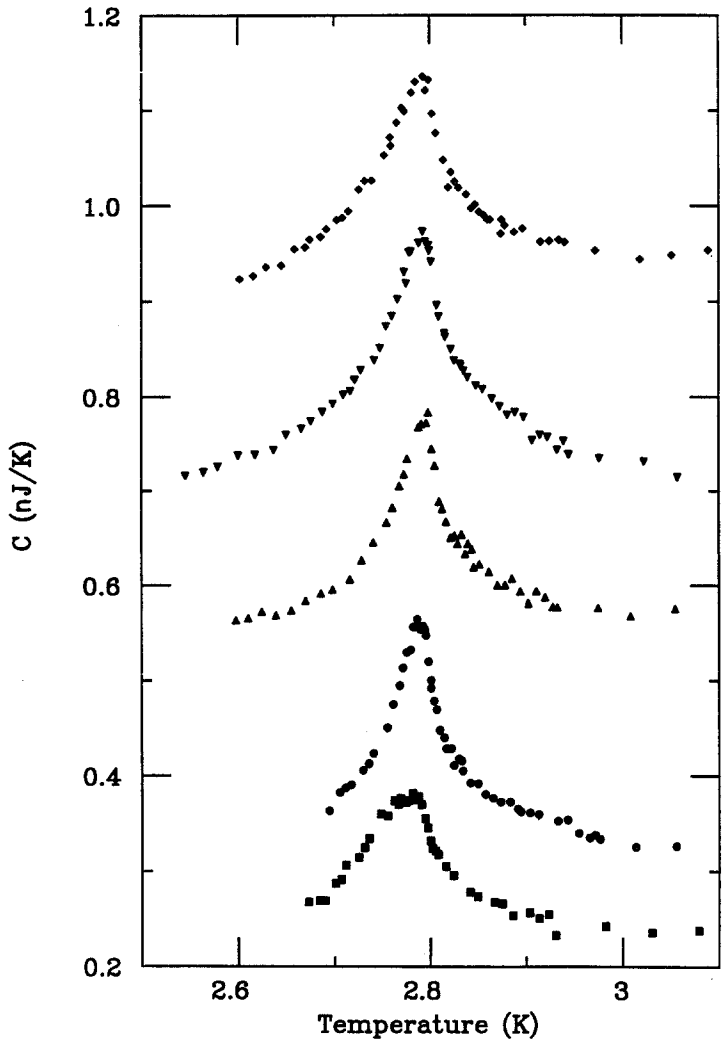

Fig. 5. Reduced heat capacity of ordering peaks for Set II as explained in text. Vertical offsets are +0.0, 0.10, 0.40, 0.55, and 0.75 nJ/K for runs taken on 7/01 (■), 6/28 (●), 6/27 (▲), 6/26 (▼), and 6/24 (◆), respectively.

power law expression

$$C = A(t^{\alpha} - 1)/\alpha + B + ct, \qquad t = |T - T_c|/T_c \tag{5}$$

where A, B, and c are constants. The critical exponent α tended toward zero for all variations of fitting conditions (i.e., using only data above or

below T_c, deleting one or both background parameters, B and c, deleting points close to T_c), or else the fits did not converge at all. It eventually become evident that the peaks of Fig. 5 are all logarithmic in shape, so we refit each side of every peak with the 3 parameter form

$$C = A \log_{10}(t) + ct \tag{6}$$

Resulting parameters and their uncertainties are given in Table I for fits spanning at least a decade in $|t|$. They include heat capacity points no higher than about 0.05 nJ/K from peak maximum. This corresponds to data further than about 10 mK from T_c, much larger than the <1 mK ac temperature oscillations used in acquiring the data. The background parameter B is missing from Eq. (6) because in every instance, setting B to zero improved the fit by a factor of at least 10 [χ^2's became better than 0.9996; F values (regression mean square/residual mean square) were typically 20,000–30,000]. Since we took data at equal temperature increments, but for the reduced temperature fits desired an equal weighting of points along the abscissa, data points were weighted as approximately $-\log_{10}(t)$. The very small background term needed confirms that our no-peak subtraction method has considerable validity.

The evidence is that we are *not* observing a 3-state Potts model in 2D. The ordering temperature is very different from $T_c = 2.93$ K expected from experiments on exfoliated graphite[1,2] and α is about 0, not 1/3 as predicted from theory.[3] Tejwani, Ferreira, and Vilches found that an ordered phase of helium adsorbed on argon plated graphite also exists.[10] Its phase diagram has an n_c which is identical to that for helium on bare graphite, but critical melting occurs at 3.113 K. The heat capacity anomaly is a logarithmic divergence characteristic of a 2-state Potts (or Ising) model. The physical

TABLE I

Critical Parameters and Uncertainties of Logarithmic Fits Made for Set II Data Using Eq. 6[a]; Run Numbers Refer to Run Dates

Runs	A^+	c^+	T_c^+	A^-	c^-	T_c^-	A^+/A^-
6/22	−0.1554	0.9620	2.7924	−0.1658	−0.0996	2.7863	0.937
	±0.0023	±0.0600	±0.0019	±0.0021	±0.0300	±0.0018	
6/24	−0.1393	0.6190	2.7924	−0.1393	−0.3150	2.7859	0.858
	0.0012	0.0300	0.0009	0.0011	0.0240	0.0041	
6/26	−0.1409	0.0074	2.7920	−0.1619	−0.1040	2.7826	0.800
	0.0041	0.0020	0.0014	0.0023	0.0400	0.0016	
6/27	−0.1257	0.3800	2.7947	−0.1280	0.1360	2.7779	0.982
	0.0025	0.0710	0.0020	0.0023	0.0680	0.0015	
6/28	−0.1704	0.5550	2.7849	−0.1789		2.7840	0.952
	0.0025	0.0490	0.0021	0.0018		0.0018	

[a] "+/−" refer to temperatures above/below T_c.

analogy is that close-packed monatomic molecules present a hexagonal mosaic for overlayer adsorption, allowing (with *nn* exclusion) only two equivalent triangular adsorbate lattices to form. Therefore, we conclude that *our single leaf calorimeter was not yet free of impurities and helium ordered on top of residual (probably monolayer thickness) adsorbates.* That we see T_c at some other temperature than 3.113 K (i.e., 2.79 K) only means that a preplated gas is present on the surface at some lightly different areal density than used in Ref. 10.

Looking more carefully at the critical parameters for the Set II fits of Table I, we note that the T_c^+ is about constant for four closely spaced coverages (6/22-6/27) but starts to fall for the 6/28 run and by 7/01 has broadened and shifted appreciably (see Fig. 5). This trend is consistent with the ^{4}He/Ar/Gr phase diagram.[10] We note, however, that the T_c^-'s determined from the critical fits are about 10 mK lower than the corresponding T_c^+ and that the ratio A^+/A^- is close to 1. Tejwani *et al.* report $A^+/A^- \simeq 0.45$ for their highest peak, while theoretically, duality symmetry in two dimensions[11] forces the equality of amplitudes $A^+ = A^-$ for all α.

4.3. The Set III Data

We heated the graphite leaf ac calorimeter to 250°C (520 K), *in situ*, while regulating the cell chamber at 12 K. For heating, a 45-volt alkaline battery was connected to the cell thermometer through a 1 kΩ bias resistor. Temperatures were determined from the high-T calibration of the thermometer obtained during the original bakeout. Radiative heating from the ac calorimeter eventually raised the chamber to 15 K. After 1 day at 520 K, the battery was disconnected and the calorimeter quickly cooled back to 12 K. Since the Grafoil ballast was kept cold, the adsorbed film on it was still in near-equilibrium. We therefore followed the previous annealing procedure of 4–5 hours at 10 K, before making a slow cooldown to the bath temperature over another 3 hours.

Heat capacity scans were taken at each 1% variation in coverage, to as much as 15% away from out Set II ordering coverage. Only monotonic signals were obtained, inferring that our heat treatment was still insufficient. We then reheated *in situ* for another day, but this time raised the ac calorimeter to about 300°C (573 K), followed by the cooldown procedure.

We again searched for the ordering peak, eventually finding it, but at a coverage 5% *lower* than that observed for Sets I and II. Evidently, evaporation and/or surface migration of impurities caused the coverage shift through an increase in helium adsorption potential on the cleaned, rather than on the impurity covered graphite leaf calorimeter. (In order for the calorimeter and ballast to equilibrate at a single chemical potential value

after the *in situ* baking, slightly more helium would be adsorbed on the leaf than for set II. To correct back to the critical coverage on the calorimeter, a measurable quantity of gas would have to be removed from the Grafoil ballast, thus lowering the measured coverage.)

A crucial indicator of graphite surface integrity is observation of an ordering peak at the expected temperature. Our Set III run of 8/6 showed a T_c of about 2.93 K, confirming adequate surface preparation. We thus continued with a full set of heat capacity runs at coverages near 215 Torr/Hg, followed by a final careful resistor calibration on 8/23 prior to warmup. Over the course of our experiment which included four resistor calibrations, the germanium cell thermometer parameter A shifted down by about 5%, while R_0 and B in Eq. (4) were stable. (For convenience, we will henceforth refer to our Set III run dates as run #'s. Thus, the run taken on 8/06 will become #06.)

Upon analyzing our data with the Set III calibration fit parameters, we found that the heat capacity data away from the ordering peak did not exactly overlap for the various runs. We eventually noticed that the ($<7\%$) heat capacity variations correlated with the date of the data run. It seemed clear that our thermometer was not completely stable with time, even when kept below 10 K, but drifted slowly during the 16-day acquisition period of the Set III data. Fortunately, the effect of the drift on the heat capacity could be compensated for quite readily.

Since our last data set, #22, was taken only one day prior to calibration, we renormalized the heat capacity values of all the other runs to #22 both at 3.20 K and at 4.20 K (renormalizations given in Table II). The implied assertion that the high-temperature heat capacity tails of the ordering peaks are coverage independent in the narrow coverage range explored is consistent with earlier ^{4}He data taken on both Grafoil[1] and *ZYX* graphite.[2] The results of applying these near-unity rescaling multipliers was to produce the adjusted Set III data curves shown in Fig. 6. The plot is universal, not just at the renormalization temperatures, 3.2 K and 4.2 K, but at all temperatures away from the ordering peak. Except for one run, #14, *all* of the heat capacity data agree at 2.7 K, well below the ordering peak region. Thus, the adjustment procedure has effectively corrected for our thermometer drift during the Set III data taking period. This multiplicative correction will not affect our later critical analysis of the data because the temperature dependent part of the correction is $<1\%$ of the total heat capacity in the critical region $|t| < 0.1$.

Also shown in Fig. 6 is an empty calorimeter run taken between *in situ* bakings. The data, which were reduced using the Set III calibration parameters uncorrected for thermometer drift, are well-represented by a straight line at high T (inset to Fig. 6) and an exponential fit below 3.7 K (dotted

TABLE II

Multipliers Used to Correct Set III Heat Capacities for Resistor Drift (See Text for Explanation)

August Date	Correction Multiplier
#6	$0.873+0.062T$
#7	$0.867+0.062T$
#8	$0.8195+0.080T$
#11	$0.860+0.061T$
#12	$0.855+0.061T$
#13	$0.846+0.060T$
#14	$0.928+0.040T$
#17	1.068
#21	0.981
#22	1.000
#23	Calibration Run $A=2.24$, $B=3.5$, $R_0=2.8\,\text{k}\Omega$

lines in Fig. 6). The difference between the empty calorimeter and the Set III data is about 0.4 nJ/K at temperatures well above the ordering peaks. From geometry we expected about 0.18 nJ/K, so the thermometer-heater side of the graphite leaf apparently also contains 2D gas-like adsorbed ^{4}He. Because the exact heat capacity signature of the reverse side adsorbate is not known, the empty calorimeter run requires a large, poorly determined thermometer drift correction, and since only changes in heat capacity signature at ordering are of interest for this study anyway, *we choose to remain with heat capacities, rather than specific heats, for our further analysis.* (An analysis involving a direct subtraction of the empty calorimeter data fit would be misleading since continued *in situ* baking after taking the empty calorimeter data undoutedly changed the thermometer/heater calibration parameters.)

We fit the absorption high-temperature heat capacity data with $0.392T^2-0.919$ nJ/K (inset to Fig. 6) and approximated the lower temperature data away from the peak with $0.0733T^3+0.683$ nJ/K (solid line Fig. 6). Such a T^3 to T^2 crossover in the temperature dependence of the heat capacity has been measured for bulk graphite near 3 K[9], so the crossover should, and does, appear in our cleaved graphite leaf calorimeter data.

The T^3 polynomial fit of Fig. 6 was subtracted from each of the runs of Set III. The fit provided a convenient, smoothly varying background about which coverage variations in the ordering peak size and shape could

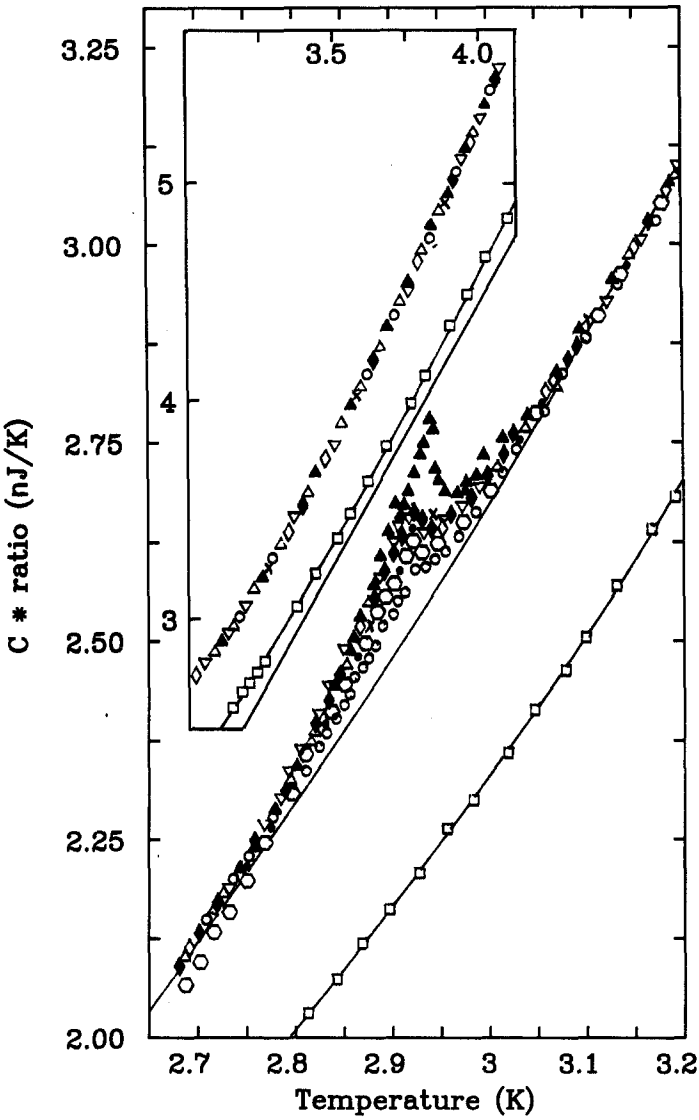

Fig. 6. Combined Set III heat capacity data corrected for thermometer drift (ratio is multiplier from Table II). Higher temperature data is shown in the inset. Representative points for runs: #07 (◆), #08 (▲), #11 (▽), #12 (◇), #13 (△), #14 (⬡), #17 (○), #21 (×), #22 (●). Empty run (not drift corrected) taken on 8/05 (□) is also shown for approximate comparison.

be compared. The final data were also three-point weighted averages* because the large magnification factor implicit in our data subtraction revealed a noticeable least significant bit roundoff error.

We present our ordering peak curves in Figs. 7 and 8, remembering that the magnitude of the heat capacity at 3.2 K is constrained to be zero. Figure 7 contains two data runs, #12 and #22, which were taken at the identical coverage of 215.25 Torr, but 10 days apart. The figure demonstrates the excellent reproduceability of our data for temperatures in the peak region and below. Clearly, the thermometer drift corrections applied to the #12 data were appropriate. There is, in addition, a shoulder residual on the #12 data relative to the #22 run above 2.95 K. This feature seems

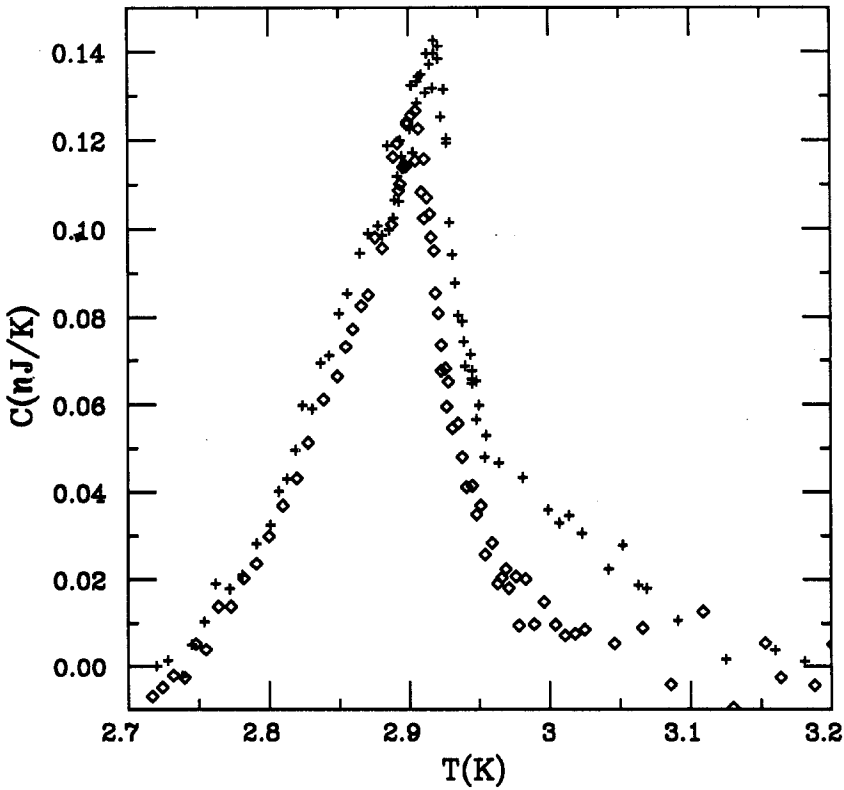

Fig. 7. Background subtracted peaks for #12 (+) and #22 (◇). Data has been three-point averaged.

*The weights of a point's two neighbors are proportional to their proximity to the point being weighted.

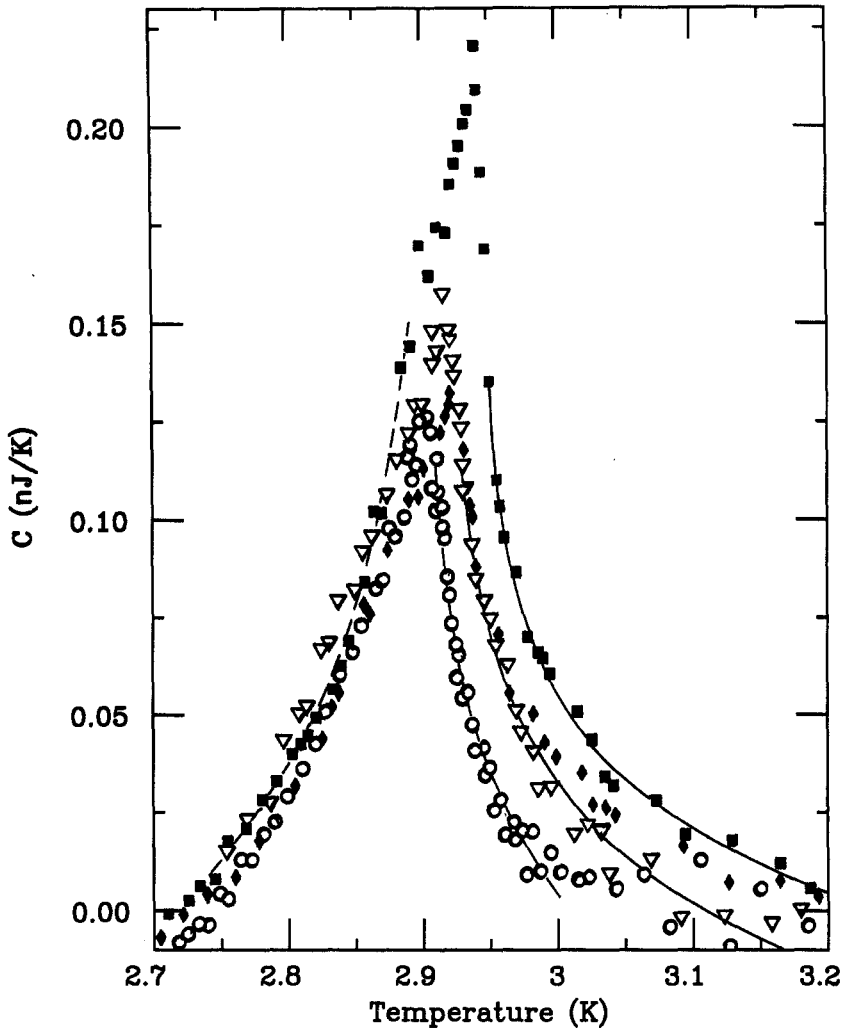

Fig. 8. Ordering peaks for #07 (◆), #08 (■), #11 (▽) and #22 (○). (Data has been averaged and background subtracted.) Lines through the data are best fit curves (see text).

unique to run #12 and is probably related to a residual annealing perturbation. Another check for annealing was to retrace data in the peak region. The #12 data, for instance, was taken for slowly decreasing temperatures, but then at 2.88 K, the cell temperature was reset to 2.95 K and after waiting a few hours, we commenced the remainder of the low-T run. There exists complete overlap of the two data subsets for run #12. Other runs (#13,

#14, and #17) which were anomalous in either background or peak strength (see Fig. 6) also showed subtle heat capacity annealing problems in the peak region. These we have discarded from further analysis.

To compare with other data, the fully averaged #22 data points are reproduced in Fig. 8 (note scale change). Our largest, sharpest peak at 214.3 Torr taken on #08 (Fig. 8) is much bigger than the #12 peak and has a higher T_c. Notice that the data nearly overlap below 2.9 K, but that at higher T (where one would expect near agreement between data sets due to the 3.2 K constraint), a large temperature shift is apparent. Two further runs are presented in Fig. 8. These are runs #07 and #11 with coverages of 213.8 and 214.9 Torr, respectively. They are each about 0.25% in coverage from the largest peak and are comparable in shape, height, and T_c. The #11 data between 2.90 K and 3.00 K is actually two passes through the peak region. Taken together, the data trend is: no change in heat capacity on the low-temperature side of all ordering peaks, a strong shift in the high-T side, growth in peak height and in T_c as coverage increases to n_c, then a height decrease and reduction in T_c as coverage goes very slightly beyond n_c.

5. ANALYSIS

An extensive critical analysis was performed to determine the shape of these heat capacity peaks. In every instance, fitting with the general power law form of Eq. (5) using a constant background B and equal weighting of data points gave either no convergence at all, or else gave such large errors for α and such poor overall fits that we are certain that none of the peaks of Fig. 8 are power laws. We did obtain good convergence and fair results for $t > 0$ with logarithmic fits, which are the superimposed lines on the data of Fig. 7. The fit parameters for these Set III curves are given in Table III. The lines in the figure extend only as far as the data

TABLE III

Critical Parameters from the Set III Fits

	A^+	B^+	T_c^+	A^-	B^-	T_c^-	A^+/A^-
#08	−0.01416	−0.075	2.9461	−0.0261	−0.179	2.9117	0.543
	±0.0005	±0.004	±0.0009	±0.0017	±0.011	±0.0036	
#11	−0.0163	−0.103	2.9222				
	±0.009	±0.007	±0.0020				
#22	−0.0185	−0.14	2.9035				
	±0.0017	±0.01	±0.0022				

used for the respective fits and do not include regions of peak rounding and/or slight nonequilibration.

Figure 9 gives the corresponding logarithmic plot of the #08 $t > 0$ data using $T_c = 2.9461$ K, obtained from the fit of the averaged data (dotted line in Fig. 8, $\chi^2 = 0.994$, F value = 1371). The fit shown in Fig. 8 extends over almost 2 decades in reduced temperature, comparable to that obtained by Bretz[2] on ZYX and CB[4] on HOPG surfaces. Peak rounding occurs within

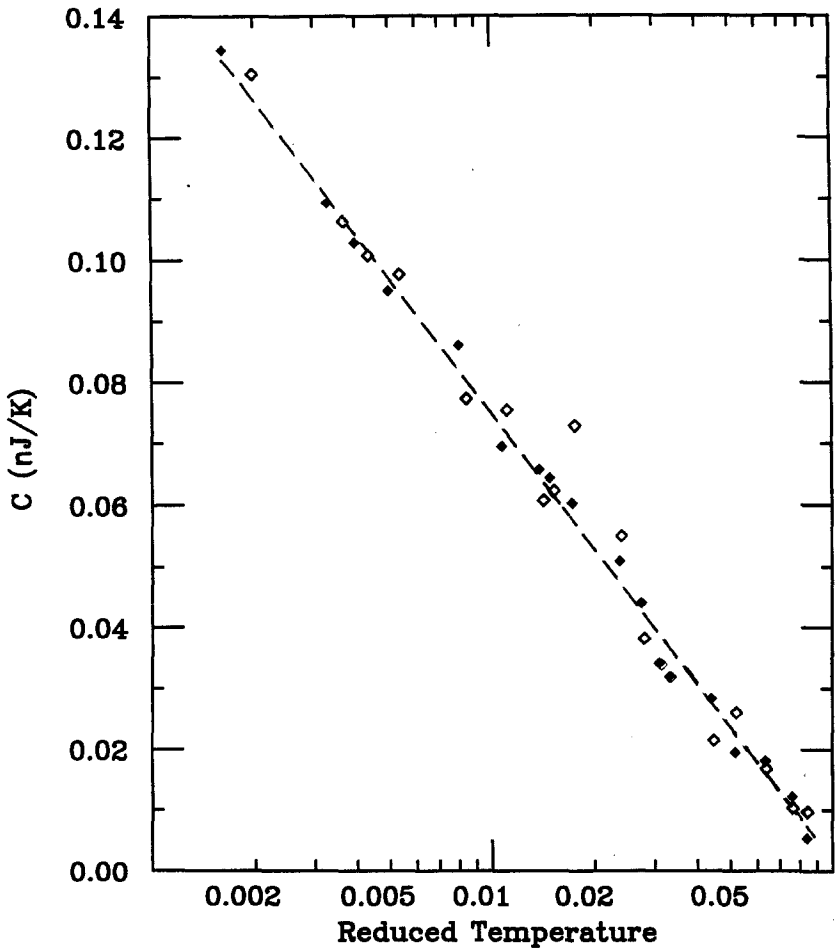

Fig. 9. Logarithm of heat capacity vs. reduced temperature for #08 (highest peak) data. Averaged data (◆, $T_c = 2.9461$ K), unaveraged data (◇, $T_c = 2.9450$ K). Best fit for (◆) given by line. $T_{ac} < 1$ mK for unaveraged data points.

$t = 0.001$, indicative of lateral crystallite sizes at least as large as those inferred from ^{4}He ordering on HOPG or *ZYX* substrates.

The open symbols represent the original data points with T_c determined by a previous fit to the unaveraged data. For this fit Efron's Bootstrap technique was used to reduce the importance of outlying data points, thereby reducing errors in the critical parameters.[12] Although still resulting in somewhat larger parameter uncertainties than for the averaged data, the earlier fit does encompass the fit parameters of Table III. Since the unaveraged data also fall along the dotted line in Fig. 8, the averaging process *does not* distort our critical analysis. Neither do our resistor drift corrections affect the analysis. Inspection of Figs. 7 and 8 with the corresponding figures for data reduced in an entirely different way[7] show the same respective T_c's, to within a few millidegrees.

Another concern was that choosing a (T^3 + constant) background subtraction might have prejudiced the outcome of our critical analysis. We therefore resubtracted a representative alternative background of (T^2 + constant) from the #08 (highest peak) data. The peak heat capacity did grow by 0.03 nJ/K, with stationary wings at 3.2 K and 3.6 K, giving a weaker divergence, yet preserving the approximately logarithmic character of the peak. Using other, more extreme functional forms for the background could conceivably have altered our critical analysis. However, since a change from $\alpha = 0$ to $\alpha = 1/3$ requires a very significant peak sharpening, we believe that a 3-state Potts divergence must be ruled out.

A $t < 0$ fit was also made for the #08 data. We found that $T_c^- = 2.9117$ K does not agree with $T_c^+ = 2.9461$ K although $A^+/A^- = 0.54$ is close to that found for the ^{4}He ordering on *ZYX* at n_c^3. The nonagreement in T_c is perhaps related to an anomaly near 2.900 K and 0.18 nJ/K. This feature could be caused by one small region of the film still not quite in equilibrium, and thus having a density slightly different from n_c. It also could be that the anomaly is just scatter, and that the low-temperature peak shape is slightly cusped rather than a logarithmic divergence. In fact, the data for all runs of Fig. 8 are consistent with straight lines from about 2.82 K up to their respective T_c's. (With the alternate T^2 + const. background subtraction the linearity would be extended to even lower temperatures.)

6. INTERPRETATIONS

Fisher renormalization has been shown to explain severe peak rounding for constant coverage heat capacity runs near, but not at, n_c.[13] Constant coverage runs slightly off of n_c have a temperature-dependent chemical potential which can renormalize peaks at n_c, with $\alpha = 1/3$ for example, into logarithmic divergences or even cusps, far enough away from n_c. When

plotted vs coverage, our Set III peak temperatures give a reasonable phase diagram for the ordered region (Fig. 10), insuring that we have actually sampled in the near vicinity of n_c, where an unrenormalized and/or some partially renormalized heat capacity peaks should exist. However, we find no strongly divergent peaks at all.

In Fig. 10, the small vertical error bars represent uncertainties associated with determinations of $T_c(>)$ as recorded in Table III, while the larger bars come from visual estimates for those coverages not analyzed for their critical parameters. For #08 the average (■) of $T_c(>)$ and $T_c(<)$ is also shown in Fig. 10. The horizontal error bars represent relative gas metering accuracy. In the narrow coverage window of Set III (<1% coverage variation) the phase boundary between ordered and higher temperature 2D fluid phases is very sharp on both sides of $n_c \simeq 214.3$ Torr. (Peak heights versus coverage for our data are shown in the inset of Fig. 10. Except for a clearly anomalous point #17, peak height variations follow the trend of the phase diagram.)

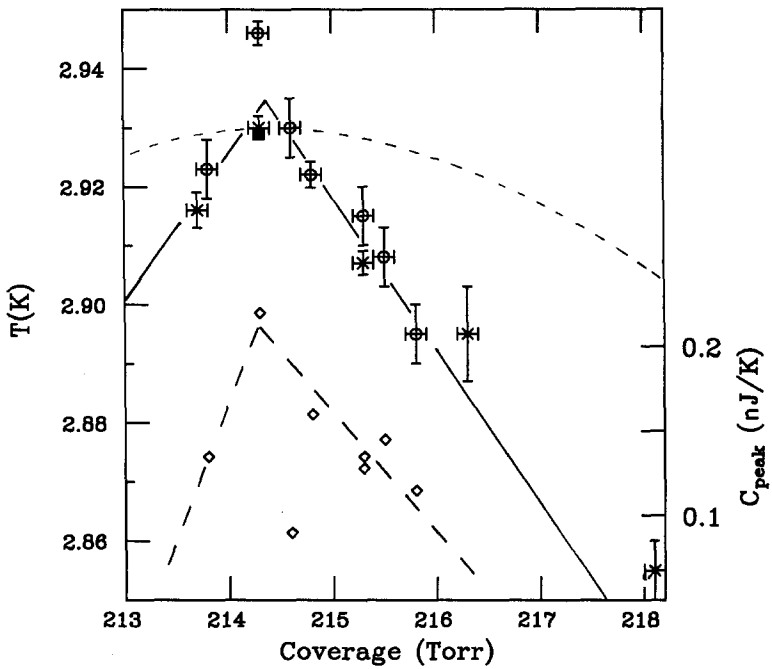

Fig. 10. Phase diagram from Set III data (○, $T_c(>)$) and from Ref. 4 (×, data downshifted by 4.2%). ■ is average T_c for run #08. Dotted line represents commensurate phase boundary as determined on various exfoliated graphites. Inset: peak heights vs. coverage. Solid line for $n < n_c$ is theoretical prediction,[14] solid line above n_c and dashed line are guides for the eye ($n_c = 214.3$ Torr $= 0.0634/\text{A}^2$).

For comparison, the Campbell and Bretz[4] T_c points on HOPG are also plotted (x, in Fig. 10). Their points and vertical error bars encompass an average of T_c^+ and T_c^- values. Their data needed shifting by only 9.2 Torr to bring the phase diagrams into excellent agreement (see horizontal scales of Fig. 10. Remember, our experiment shared the same Grafoil ballast as the CB microcalorimeter).

Recently, de Mello *et al.*[14] performed a Migdal-Kadanoff real-space renormalization group transformation for the Potts lattice gas and predicted a phase diagram for ^{4}He and ^{3}He on graphite. De Mello found a narrower phase region for ordering than did earlier theoretical determinations[15] which considered only *nn* repulsive energies (but happened to agree pretty well with the exfoliated graphite results). It is unclear how much theoretical simplifications affect de Mello's slope determination, but his published predictions do closely agree with our measurements. The dotted straight line for $n > n_c$ in our Fig. 10 phase diagram is determined from the slope of de Mello's phase boundary where it intercepts n_c. Although our phase boundary is poorly determined for $n < n_c$, his slope is precisely the negative slope of our well-determined phase boundary for $n > n_c$, and phase diagrams should be symmetrical around critical points.

There are enough significant differences in substrate geometry between the exfoliated graphites Grafoil, Foam, and *ZYX*, and the cleaved surfaces of HOPG and single graphite crystals, that the narrowing of the ordered phase diagram and our loss of the $\alpha = 1/3$ divergence in the heat capacity should be reconcilable with the earlier work. In exfoliates, wedge-shaped adsorption chambers form as basal plane surfaces part during deintercalation. Such geometrical features result in a distribution of energy sites for gas adsorption.[16] An inherently narrow phase diagram of a highly compressible fluid should be particularly sensitive to lateral energy variations because they create a density nonuniformity within the monolayer adsorbate. Thus, the effect on ^{4}He ordering is to widen the coverage region over which commensuration occurs. The slab geometry of cleaved crystals lacks the three dimensional network of exfoliate adsorption chambers and thus eliminates this sizeable contribution to the distribution of energies. It is therefore significant that both the CB study on HOPG and the present work find a very narrow ordered phase region.

Although slab geometry is obtained upon cleaving, gold decoration of HOPG reveals, in addition to closely spaced parallel step planes, a cross-net of smaller step planes and atomic scale defects.[5,17] These might act as nucleation regions in the vicinity of which ordered phase solids can stabilize. They also act as regions where residual impurities can collect if not fully desorbed from the surface. Campbell and Bretz acknowledged that residual impurity problems of their 170C *in situ* baked cell probably affected the critical parameter α of their ordering peak, making it appear nonuniversal.

With our present cell the impurity scenario is a much less likely reason for peak shape modification. We baked at a considerably higher temperature (600 K) then did CB and our adsorption surface, natural single crystal graphite, is much more nearly ideal than cleaved HOPG surfaces. Gold decoration shows widely spaced parallel step planes with no cross-net of smaller planes and very few defects.[5] If nucleation phenomena were responsible for our quasilogarithmic ordering peak shapes, then that nucleation would most likely occur at the parallel step planes along the surface (which from mechanical scanning appear to be about 1 μm in height).

It is possible that the particular crystalline direction of the step edges could prejudice the helium/graphite ordered phase toward an Ising-like logarithmic peak. We note, therefore, that step edges occurring along the graphite basal plane lattice vectors **a** or **b** would permit edge nucleation of 3 equivalent triangular sublattice configurations, whereas step edges lying along the $R30°$ directions would only nucleate a single $\sqrt{3}\times\sqrt{3}$ $R30°$ sublattice configuration. Thus, the $R30°$ step edges could discourage domain wall pinning. We do not know in which direction step edges form on graphite, but should the effect of nucleation be important far from these edges, the character of the ordering heat capacity peak could change appreciably. This eventuality would still permit the appearance of Potts ordering peaks on surfaces possessing a variety of nucleating centers and edges (i.e., *ZYX* and HOPG).

It is well known that HOPG is a poor substrate for LEED measurements. However, using (superior quality) Kish graphite Cui and Fain[18] observed asymmetric LEED patterns at the start of adsorption experiments designed to explore the uniaxial incommensurate phase transition of monolayer hydrogen films. The asymmetry shows that one of the three equivalent uniaxial directions is nucleated much more readily than the other two and that direction is always the same. They tentatively concluded that a greater number of steps exist along a particular graphite direction, that nucleation of hydrogen films occur along these steps and that edge adsorption provides a preferential direction for further adsorption. Later, as impurities change the nucleation characteristics, a much more symmetrical pattern emerges. Since the uniaxial phase is $\sqrt{3}$ $R30°$ commensurate in one direction, we conclude that step plane edges on single crystal graphite actually do occur mostly along the $R30°$ direction.

As evidence that edge effects might indeed be altering our ordering transition, we note that our Fig. 8 possesses heat capacity features similar to the triple point melting peaks of neon monolayers on graphite.[19] There, melting into 2D liquid at 0.45 and 0.57 monolayers show exact peak overlap on the low-temperature side of the triple-point peak. It is demonstrated that edge melting of the solid neon causes a significant upward temperature shift of the high-T side of the neon peak with coverage. An energy spread

of substrate potential accounts for the peak width in the neon first-order transition and lateral energy variations close to edges account for the temperature shift at melting. The temperature shift of our data, shown in Fig. 8, is about as pronounced as in Ref. 19, while the low-T tails of all our peaks overlap with each other. The result is an increase of peak entropy as coverage approaches n_c from either side. We interpret this entropy increase as reflecting a lateral growth of the ordered phase in the vicinity of n_c.

To convincingly demonstrate that edge influence is actually constraining domain wall movement and controlling the fraction of the helium film undergoing ordering requires further experimental and theoretical study. Numerical modeling of edge constraint to ordering should be straightforward, given that the ^{4}He/graphite basal plane potential is already well known.[20] One must bear in mind that the very narrow phase diagram for ordering of helium on single crystal graphite (Fig. 10) means that the high zero-point energy and weak interaction of helium atoms keeps them from ordering except at a very specific areal density. This makes nucleation induced density variations must more important for helium than for other adsorbates.

7. CONCLUSIONS

We have reported ordered phase transition heat capacity measurements for ^{4}He adsorbed on cleaved, single crystal graphite. Through a series of successively more careful data taking sets, we have obtained heat capacity peaks of sufficient quality that conclusions regarding the nucleation of helium ordering on graphite can be ventured.

While peaks of Set II obtained on a partially cleaned surface were logarithmic in shape due to the probable presence of an inert gas overlayer, the quasilogarithmic shape of the Set III data on the 300°C *in situ* baked cell was unanticipated. These results suggest that the nature of the helium ordering transition is strongly affected by the presence of graphite surface step planes in the $R30°$ direction. Theoretical and computer modeling calculations testing this premise appear to be in order.

ACKNOWLEDGMENTS

We thank J. H. Campbell for discussions on technical aspects of ac calorimetry and The Rackham School of Graduate Studies for partial financial support.

REFERENCES

1. M. Bretz and J. G. Dash, *Phys. Rev. Lett.* **27**, 647 (1971).
2. M. Bretz, *Phys. A* **12**, 1857 (1979).
3. M. denNijs, *J. Phys. A* **12**, 1857 (1979).
4. J. H. Campbell and M. Bretz, *Phys. Rev. B* **32**, 2861 (1985).
5. J. H. Cambpell, Thesis, University of Michigan, 1985 (unpublished), and private communication.
6. P. F. Sullivan and G. Seidel. *Phys. Rev.* **173**, 679 (1968).
7. H. B. Chae, Thesis, University of Michigan, 1987 (unpublished).
8. Y. Sakai and K. Takahashi, *Jpn. J. Appl. Phys.* **2**, 629 (1963), M. Seki and K. Sanokawa, *Cryogenics* **22**, 121 (1982), M. Regelsberger, R. Wenhardt, and M. Rosenberg, *Rev. Sci. Instrum.* **58**, 276 (1987).
9. D. J. C. van der Hoeven, Jr., and P. H. Keesom, *Phys. Rev.* **130**, 1318 (1963); B. T. Kelley, Physics of Graphite (Applied Science, London, 1981).
10. M. J. Tejwani, O. Ferreira and O. E. Vilches, *Phys. Rev. Lett.* **44**, 152 (1980).
11. M. Kaufman, *Phys. Rev. B* **30**, 413 (1984), S. I. Chase and M. Kaufman, *Phys. Rev. B* **33**, 239 (1986).
12. S. B. Crary and D. A. Fahey, *Phys. Rev. B* **35**, 2102 (1987).
13. R. E. Ecke, Q. S. Shu, T. S. Sullivan, and O. E. Vilches, *Phys. Rev. B* **31**, 448 (1985).
14. E. V. L. de Mello, preprint; G. M. Carneiro and E. V. L. de Mello, *Phys. Rev. B* **35**, 358 (1987).
15. M. Schick, J. S. Walker, and M. Wortis, *Phys. Rev. B* **16**, 2205 (1977).
16. R. E. Ecke, J. G. Dash and R. D. Puff, *Phys. Rev B* **26**, 1288 (1982).
17. M. Bretz and Roy Clarke, *Phys. Rev. Lett.* **55**, 2506 (1985); G. R. Hennig, in *Chemistry and Physics of Carbon*, Vol. 2, P. L. Walker, ed. (Dekker, New York, 1966) p. 1.
18. J. Cui and S. C. Fain, Jr. *Phys. Rev. B* **39**, (to be published).
19. Da-Ming Zhu, D. Pengra and J. G. Dash, *Phys. Rev. B* **37**, 5586 (1988).
20. M. W. Cole and F. Toigo, *Phys. Rev. B* **23**, 3914 (1981).